Amino acid-based supramolecular chiral hydrogels promote osteogenesis of human dental pulp stem cells via the MAPK pathway

Peilun Li [a,d,1], Qiaoqiao Jin [a,d,1], Kangrui Zeng [a,d], Chenguang Niu [a,d], Qianyang Xie [c], Ting Dong [a,d], Zhengwei Huang [a,d,*], Xiaoqiu Dou [b,**], Chuanliang Feng [b,***]

[a] Department of Endodontics, Shanghai Ninth People's Hospital, Shanghai Jiao Tong University School of Medicine, College of Stomatology, Shanghai Jiao Tong University, Shanghai, China
[b] State Key Lab of Metal Matrix Composites, School of Materials Science and Engineering, Shanghai Jiao Tong University, Shanghai, China
[c] Department of Oral Surgery, Shanghai Ninth People's Hospital, Shanghai Jiao Tong University School of Medicine, College of Stomatology, Shanghai Jiao Tong University, National Center for Stomatology, National Clinical Research Center for Oral Diseases, Shanghai Key Laboratory of Stomatology, Shanghai, China
[d] National Center for Stomatology, National Clinical Research Center for Oral Diseases, Shanghai Key Laboratory of Stomatology, Shanghai, China

A B S T R A C T

Critical-size defects (CSDs) of the craniofacial bones cause aesthetic and functional complications that seriously impact the quality of life. The transplantation of human dental pulp stem cells (hDPSCs) is a promising strategy for bone tissue engineering. Chirality is commonly observed in natural biomolecules, yet its effect on stem cell differentiation is seldom studied, and little is known about the underlying mechanism. In this study, supramolecular chiral hydrogels were constructed using $_{L/D}$-phenylalanine (L/D-Phe) derivatives. The results of alkaline phosphatase expression analysis, alizarin red S assay, as well as quantitative real-time polymerase chain reaction and western blot analyses suggest that right-handed D-Phe hydrogel fibers significantly promoted osteogenic differentiation of hDPSCs. A rat model of calvarial defects was created to investigate the regulation of chiral nanofibers on the osteogenic differentiation of hDPSCs *in vivo*. The results of the animal experiment demonstrated that the D-Phe group exhibited greater and faster bone formation on hDPSCs. The results of RNA sequencing, vinculin immunofluorescence staining, a calcium fluorescence probe assay, and western blot analysis indicated that L-Phe significantly promoted adhesion of hDPSCs, while D-Phe nanofibers enhanced osteogenic differentiation of hDPSCs by facilitating calcium entry into cells and activate the MAPK pathway. These results of chirality-dependent osteogenic differentiation offer a novel therapeutic strategy for the treatment of CSDs by optimising the differentiation of hDPSCs into chiral nanofibers.

1. Introduction

Critical-size defects (CSDs) of craniofacial bones caused by inflammation, tumour resection, and trauma do not heal spontaneously [1], resulting in aesthetic and functional complications that seriously impact the quality of life. Traditional approaches for the treatment of CSDs often utilise autologous or allogeneic bone grafts, metals, or other synthetic materials for bone augmentation. However, the lack of predictable biological responses and limited availability restrict the clinical applications of these tissues [2]. Bone tissue engineering (BTE) by transplantation of viable stem cell (SC)-based biomaterials is a strategic method to meet clinical demands [3]. Human dental pulp stem cells (hDPSCs) have received attention as an easily accessible source of mesenchymal stem cells (MSCs) with a capacity for multidirectional differentiation [4,5], which is related to the recovery of bone, cartilage, as well as hard and soft dental tissues. Because of the higher cloning and proliferation potential of hDPSCs compared to those of bone marrow stem cells (BMSCs) [6,7], they are widely considered for application in BTE [8,9]. The osteogenic differentiation of hDPSCs can be regulated by biochemical factors such as growth factors and hormones [10–12] but is

---

limited by stability, release sustainability, inflammation, and ectopic bone formation [13]. Therefore, many studies have focused on the development of exogenous growth factor-free scaffold materials that can regulate biological activities [14–17]. To achieve sufficient regenerative capacity, it is essential to ensure that the physical properties of the complex native microenvironment promote cell differentiation [18–21]. Natural biomolecules are chiral compounds that self-assemble into cells and the extracellular matrix (ECM) with three-dimensional chiral structures [22–24]. Therefore, developing ECM-mimicking biomaterials with chiral properties is crucial for stimulating tissue regeneration [15, 25].

Hydrogels are morphologically adaptable and suitable as scaffold biomaterials for irregular bone defects in the maxillofacial region [26]. Although chirality affects the proliferation, adhesion, and differentiation of several types of MSCs [27–32], the behaviour of hDPSCs in different chiral hydrogel scaffolds remains unexplored. Hence, it is necessary to elucidate the effects of chirality on the osteogenic differentiation of hDPSCs and clarify the underlying mechanisms for their application in BTE.

In this study, supramolecular chiral hydrogel scaffolds were constructed using two enantiomeric $_{L/D}$-phenylalanine gelators (L-Phe and D-Phe) to mimic the ECM of hDPSCs. L-Phe and D-Phe gelators can self-assemble into left-handed and right-handed helical nanofier hydrogels, respectively. Meanwhile, a racemic mixture of L-Phe and D-Phe gelators (R-Phe) formed nonhelical hydrogel nanofiers. The right-handed D-Phe hydrogel significantly promotes osteogenic differentiation of hDPSCs. RNA sequencing (RNA-seq), quantitative real-time polymerase chain reaction (qRT-PCR), immunofluorescence, and western blot analyses were performed to clarify the molecular mechanisms employed by the chiral supramolecular hydrogels to promote the osteogenic differentiation of hDPSCs. The results of the RNA-seq analysis showed that left-handed L-Phe fibers affected pathways involved in the formation of tight junctions between cells, whereas right-handed D-Phe fibers upregulated calcium signalling and fatty acid metabolic pathways, which are associated with osteogenic differentiation. Furthermore, immunofluorescence staining of vinculin, a membrane-cytoskeletal protein that forms focal adhesions, the use of a fluorescent probe to detect calcium, and western blot analysis confirmed that L-Phe fibers enhanced the adhesive capacity of hDPSCs, whereas D-Phe fibers promoted the entry of calcium into cells and the subsequent activation of the mitogen-activated protein kinase (MAPK) signalling pathway. The ability of chiral supramolecular hydrogels to promote the osteogenic differentiation of hDPSCs has potential applications in the treatment of craniofacial bone defects.

2. Materials and methods

2.1. Synthesis of L/D-Phe gelators and preparation of chiral hydrogels

L/D-Phe gelators were synthesised as previously described [33]. The hydrogels (0.5 mg/mL) were prepared using a heating-and-cooling method [31,34,35]. First, L-Phe, D-Phe, or L-Phe + D-Phe molecules were suspended in water at room temperature, then heated to 95 °C to form a clear solution, and cooled to room temperature to form a gelatinous material, which was transferred to plates and placed at 60 °C oven (Thermo) for 12 h. The cell suspension was added to a plate containing the hydrogel. For animal experiments, we mixed hDPSCs with Dulbecco's modified Eagle's medium (DMEM) into a concentrated solution of the gelator (final gelator concentration: 5 mg/mL) in DMSO (final DMSO concentration: 4.0 %) (Fig. S1).

2.2. Characterization of materials

Proton nuclear magnetic resonance (^{1}H NMR) spectroscopy was performed using a Bruker Avance III™ HD 400 MHz spectrometer (Bruker Corporation, Billerica, MA, USA). The gels were diluted to 0.1 mg/mL and imaged using a FEI QUANTA 250 scanning electron microscope (FEI Company, Hillsboro, OR, USA). The circular dichroism (CD) spectra were recorded using a JASCO J-815 CD spectrometer (JASCO Corporation, Tokyo, Japan). Ultraviolet–visible (UV–Vis) spectra were recorded using an Evolution 201 spectrophotometre (Thermo Fisher Scientific, Waltham, MA, USA). For the CD and UV–Vis measurements, the concentration of the samples was 0.5 mg/mL. Fourier transform infrared (FT-IR) spectroscopy was performed using an Equinox 55 spectrometer (Bruker Daltonics GmbH, Bremen, Germany). The powdered samples were prepared using the KBr pellet technique.

2.3. Isolation and culture of hDPSCs

The study protocol was approved by the Ethics Committee of Shanghai Ninth People's Hospital, which is affiliated with Shanghai Jiao Tong University (approval no. SH9H-2021-TK171-1), and was conducted in accordance with the ethical principles for medical research involving human subjects described in the Declaration of Helsinki. Written informed consent was obtained from all the participants before their inclusion in the study. hDPSCs were obtained from the dental pulp of impacted third molars of patients (age, 16–22 years) and cultured in DMEM (Sigma-Aldrich Corporation, St. Louis, MO, USA) supplemented with 10 % fetal bovine serum (Sigma-Aldrich Corporation) and 1 % penicillin/streptomycin (Gibco-BRL, Gaithersburg, MD, USA) as described previously[10]. HDPSCs were cultured in an osteogenic differentiation medium (Cyagen Biosciences Co., Ltd., Guangzhou, China) to induce osteogenesis and harvested at passages 3–5.

2.4. Toxicity of chiral hydrogels to hDPSCs

The cytotoxic effects of the chiral hydrogels were evaluated by staining with calcein-AM/propidium iodide, labelling with 5-ethynyl-2′-deoxyuridine (EdU), and using the Cell Counting Kit 8 (CCK-8) assay.

For the calcein-AM/PI staining assay (Bestbio, Jiangsu, China), hDPSCs (2.5×10^4 cells per well) were cultured in triplicates in 48-well plates containing different chiral nanofiber hydrogels and DMEM for 24 h. An equal amount of cell suspension was added to a plate without the hydrogel for the control group. Afterwards, the plates were washed three times with phosphate-buffered saline (PBS), and the wells were filled with 200 μL of calcein-AM/PI working solution. Following incubation at 37 °C for 30 min, images were captured under a fluorescence microscope (BX51; Olympus Corporation, Tokyo, Japan) and then processed, and analysed using ImageJ software.

For the EdU incorporation assay (Beyotime Institute of Biotechnology, Shanghai, China), hDPSCs (5×10^4 cells/well) were cultured in triplicate in 24-well plates containing different chiral nanofiber hydrogels and DMEM until they reached 50 % confluence. For the control group, an equal amount of the cell suspension was added to a plate without the hydrogel. Afterwards, DMEM and 10 μM EdU labelling medium (1:100) were added and incubation was continued for 4 h. Then, the cells were fixed with 4 % paraformaldehyde and stained with a click reaction solution and Hoechst 33342 nucleic acid stain. Images were captured using a fluorescence microscope. The doubling rate of the cells was assessed by calculating the ratio of EdU-positive nuclei (green) to Hoechst-positive nuclei (blue) in five random visual fields.

For the CCK-8 assay, hDPSCs (1000 cells per well) were seeded in 96-well plates containing the different chiral nanofiber hydrogels. For the control group, an equal amount of the cell suspension was added to a plate without the hydrogel. After 1, 3, 5, and 7 days of incubation, 10 μL of CCK8 buffer was added to each well, and incubation was continued at 37 °C for 1 h. Afterwards, the optical density was measured at a wavelength of 450 nm using a microplate reader (Multiskan FC; Thermo Fisher Scientific).

2.5. Alkaline phosphatase (ALP) staining and quantification

ALP, an important enzyme involved in the early stage of odontogenesis, was detected using the 5-bromo-4-chloro-3-indolyl-phosphate/nitro blue tetrazolium (BCIP/NBT) alkaline phosphatase colour development kit (Beyotime Institute of Biotechnology) according to the manufacturer's instructions. Briefly, hDPSCs (5×10^4 cells per well) were cultured in triplicate in 24-well plates containing different chiral nanofiber hydrogels and osteoblast differentiation-inducing medium for 5 days. For the control group, an equal amount of the cell suspension was added to a plate without the hydrogel. Afterwards, the cells were fixed and stained with an ALP working solution at 37 °C for 20 min in the dark. The plate was then washed, and images were captured under an inverted phase-contrast microscope. For ALP activity assays, after treatment with OM for 5 days, cells were incubated with *p*-nitrophenyl phosphate (Sigma-Aldrich, St. Louis, MO, USA), and ALP activity was detected by measuring the optical density (OD) at 405 nm. The total protein content of the cells was measured using a bicinchoninic acid (BCA) Protein Assay Kit (Pierce Biotechnology, Thermo Fisher Scientific, Waltham, MA, USA), and ALP activity was expressed as OD per milligram of total protein.

2.6. Alizarin red S staining and quantification

Alizarin red S staining was performed to evaluate the influence of chirality on the capacity of hDPSCs to form calcified nodules. Briefly, hDPSCs (2×10^5 cells per well) were seeded in triplicate in a 6-well plate containing different chiral nanofiber hydrogels and osteoblast differentiation-inducing medium. For the control group, an equal amount of the cell suspension was added to a plate without the hydrogel. After 21 days of cultivation, the cells were fixed with 4 % paraformaldehyde for 30 min and stained with Alizarin Red S (Sigma-Aldrich Corporation). The cells were imaged using an inverted phase-contrast microscope. To quantify mineralisation, the stains were dissolved in 100 mmol/L cetylpyridinium chloride for 30 min, and the absorbance was determined at 562 nm. The final mineralisation levels in each group were calculated after normalising to the total protein concentration obtained from duplicate plates.

2.7. Western blot analysis

Western blot analysis was performed to assess the expression profiles of osteogenic-related markers and the role of the MAPK signalling pathway in the osteogenic differentiation of hDPSCs induced by chiral hydrogels, as previously described [30,36]. Briefly, hDPSCs were cultivated with chiral hydrogels, and osteogenic differentiation was performed for 7 days. In addition, hDPSCs cultivated with the chiral hydrogels for 12 h were collected to investigate the involvement of the MAPK signalling pathway. Total protein was extracted from cells using radioimmunoprecipitation assay buffer (Beyotime Institute of Biotechnology, Shanghai, China). Then, the cell lysates were centrifuged at 12000 rpm for 15 min at 4 °C, and the protein content was quantified using a bicinchoninic acid assay (Beyotime Institute of Biotechnology). Afterwards, the proteins were separated by electrophoresis using 10 % sodium dodecyl sulfate polyacrylamide gels and then electroblotted onto polyvinylidene fluoride membranes (EMD Millipore Corporation, Billerica, MA, USA), which were blocked with 5 % (w/v) nonfat dried skimmed milk diluted in tris-buffered saline-Tween 20 and probed with primary antibodies against dentin matrix protein-1 (DMP-1; Invitrogen Corporation, Carlsbad, CA, USA), runt-related transcription factor 2 (RUNX2; Cell Signaling Technology, Inc., Danvers, MA, USA), osterix (OSX; Abcam, Cambridge, MA, USA), p38, phospho-p38 (p-p38), p44/42 (ERK1/2), phospho-p44/42 (*p*-ERK1/2), c-Jun N-terminal kinases (JNK), phospho-JNK (*p*-JNK), and glyceraldehyde-3-phosphate dehydrogenase (GAPDH; Sigma-Aldrich Corporation) overnight at 4 °C, followed by incubation with corresponding horseradish peroxidase-conjugated secondary antibodies (Biotechwell, Shanghai, China) for 1 h at room temperature. Finally, the protein bands were visualised using an enhanced chemiluminescence kit (Merck KGaA, Darmstadt, Germany) and quantified using the ImageJ software. The expression levels of the proteins of interest were normalised to those of GAPDH.

2.8. qRT-PCR analysis

After 7 days of osteogenic induction, total cellular RNA was extracted from the L-Phe, D-Phe, R-Phe, and control groups using TRIzol reagent (Invitrogen Corporation) and reverse-transcribed into complementary DNA using the PrimeScript RT reagent kit (Takara Bio, Inc., Shiga, Japan) in accordance with the manufacturer's instructions. The expression profiles of markers of mineralisation (*DMP-1*, *RUNX2*, and *OSX*) were assessed using a SYBR Premix Ex Taq TM II Kit (Takara Bio, Inc.) and an ABI PRISM® 7500 FAST Sequence Detection System (Applied Biosystems, Carlsbad, CA, USA). The mRNA expression levels of the genes of interest were normalised against expression of GAPDH, which served as the housekeeping gene, using the $2^{-\Delta\Delta Ct}$ method. The primers used for qRT-PCR (Supplementary Table 1) were synthesised by Sangon Biotech Co., Ltd. (Shanghai, China). All samples were amplified in triplicates.

2.9. In vivo experiments with a rat model of cranial bone defects

To confirm that the chiral hydrogels induced the osteogenic differentiation of hDPSCs, a Sprague–Dawley (SD) rat model of full-thickness cranial defects was created [37,38]. Male SD rats (age, 8 weeks) were obtained from the Ninth People's Hospital Animal Center (Shanghai, China) and anaesthetised with pentobarbital sodium (1 %) before the creation of full-thickness defects on both sides of the calvarial bone. Then, hDPSCs (5×10^5 cells per well) suspended in 50 μL of L-Phe or saline (control group) (n = 10) were injected into the left defect, while hDPSCs (5×10^5 cells per well) in 50 μL of D-Phe or R-Phe (n = 10) were injected into the right defect (Fig. S2). Subsequently, a sequential fluorescence labelling method was used to monitor tissue mineralisation. Briefly, the rats were injected intra-abdominally with tetracycline (25 mg/kg; Sigma-Aldrich Corporation), calcein (20 mg/kg; Sigma-Aldrich Corporation), and Alizarin Red S (30 mg/kg; Sigma-Aldrich Corporation) at 1, 3, and 5 weeks after surgery. The rats were sacrificed 8 weeks after surgery with an overdose of anaesthetic medication. The cranial bones were harvested and fixed in 4 % paraformaldehyde for 48 h and then stored in 75 % ethanol at 4 °C for further analysis. Specimens (n = 5) were scanned using a micro-computed tomography (CT) instrument (SkyScan 1176; Bruker Optics GmbH & Co. KG, Ettlingen, Germany). The ratios of bone volume to total volume (BV/TV), bone mineral density (BMD), and mean trabecular separation (Tb.Sp) were calculated as previously described [10]. Sequential fluorescence labelling was assessed using five samples that were randomly selected from each group, embedded in polymethylmethacrylate, cut into 200 μm-thick sections with a saw microtome (Leica Biosystems Nussloch GmbH, Nussloch, Germany), further polished into 40–50 μm-thick sections, and observed under a confocal laser scanning microscope (CLSM 700; Carl Zeiss, Oberkochen, Germany) with excitation/emission wavelengths of 405/580 nm for tetracycline, 488/517 nm for calcein, and 543/617 nm for alizarin red S. Van Gieson's picrofuchsin staining was used for histological analysis. Meanwhile, five samples randomly selected from each group were decalcified in 10 % ethylenediaminetetraacetic acid on an orbital shaker at 37 °C for 4 weeks, embedded in paraffin, and sliced into 4 μm-thick sections, which were then de-paraffinised, stained with haematoxylin-eosin (HE) to detect newly formed bone, and imaged under an inverted phase-contrast microscope.

2.10. RNA-seq analysis

After 7 days of osteogenic induction, total cellular RNA was extracted from the L-Phe and D-Phe groups with TRIzol reagent (Invitrogen Corporation), purified, and reverse transcribed into complementary DNA, which was used to construct a library with the TruSeq™ DNA Library Preparation Kit (Illumina, Inc., San Diego, CA, USA). After quantification with an Invitrogen™ Qubit™ 4 Fluorometer (Thermo Fisher Scientific), paired-end reads were sequenced with the NovaSeq 6000 sequencing platform (Illumina, Inc.). The expression level of each transcript was calculated as transcripts per million reads to identify differential expression genes (DEGs) between two different samples. RNA-Seq by expectation maximisation (RSEM) software [39] was used for quality control of gene abundance. The parameters for DEGs were absolute log2 (fold change) > 1 and adjusted probability (p) value $\leq$ 0.05. Gene ontology (GO) and pathway enrichment analyses were performed using the Kyoto Encyclopedia of Genes and Genomes (KEGG) database to identify the functions of significantly enriched DEGs. The only parameter for significantly enriched GO terms and metabolic pathways was a Bonferroni-corrected *p-value* $\leq$ 0.05 compared to the whole-transcriptome background. GO functional enrichment and KEGG pathway analyses were conducted using Google and the KEGG Orthology-Based Annotation System (KOBAS) tool [40].

2.11. Immunocytochemical analysis

The effect of chiral hydrogels on the adhesive capacity of hDPSCs was evaluated. Briefly, hDPSCs (2×10^4/mL) were incubated in confocal dishes containing different chiral nanofiber hydrogels and growth medium for 24 h. Cells were then rinsed with PBS, fixed with 4 % paraformaldehyde for 20 min, and permeabilised with 0.1 % Triton X-100 for 15 min. After blocking with 5 % bovine serum albumin for 30 min, the cells were incubated overnight at 4 °C with a mouse monoclonal antibody against vinculin (dilution 1:100; Sigma-Aldrich Corporation), followed by a secondary antibody (Dako, Glostrup, Denmark) for 1 h at room temperature. The cytoskeleton was stained with fluorescein isothiocyanate-labelled phalloidin (Yeasen, China) for 1 h, and nuclei were stained with 4′,6-diamidino-2-phenylindole for 5 min. Images were obtained using a confocal laser-scanning microscope (Leica Microsystems GmbH, Wetzlar, Germany).

2.12. Detection of intracellular calcium levels

The intracellular calcium ion levels of hDPSCs were measured with diluted Fluo-4 AM ester stock solution (1 μM with PBS; Beyotime Institute of Biotechnology). Briefly, hDPSCs (2×10^4/mL) were cultured in triplicate in confocal dishes containing different chiral nanofiber hydrogels and growth medium. After 24 h, the culture medium was removed, the cells were rinsed three times with PBS, and the culture was continued in Fluo-4 AM solution at 37 °C for 30 min. The Fluo-4 AM solution was then removed, and the cells were rinsed three times with PBS and incubated for an additional 30 min. Nuclei were stained with Hoechst 33342 nucleic acid stain (Beyotime Institute of Biotechnology) and imaged using a confocal laser scanning microscope (Leica Microsystems GmbH) at excitation and emission wavelengths of 488/512 nm.

2.13. Statistical analysis

Statistical analyses were performed using Prism software (version 7.0; GraphPad Software, Inc., San Diego, CA, USA). The results are reported as the average of three independent experiments. Normally distributed data were analysed using Student's *t*-test and one-way analysis of variance (ANOVA). A *p-value* < 0.05 was considered statistically significant.

3. Results

3.1. Characterization of the materials

The L-Phe, D-Phe, and R-Phe gelators can assembled into hydrogels in water, whereas they dissolve in methanol. To observe the detailed structures, the hydrogel concentration was diluted to 0.1 mg/mL. Atomic force microscopy (AFM) and transmission electron microscopy (TEM) measurements in a previous study [41] revealed the formation of left-handed helical structures for L-Phe fibers and right-handed fibers for D-Phe assemblies. The SEM images (Figure 1a–c) confirmed that the L-Phe, D-Phe, and R-Phe hydrogels were composed of left-handed (*M*), right-handed (*P*), and non-helical nanofibers, respectively. The chiroptical activity of the hydrogels was further characterised using CD measurements. In the methanol solution, the CD signals of the L-Phe and D-Phe molecules were weak at 218 and 273 nm, respectively, while the CD signals of the R-Phe was silent (Fig. 1d). As compared to the L/D-Phe molecules, the L/D-Phe hydrogels exhibited significantly enhanced CD intensity at 229 nm and a positive CD peak at 270 nm at 0.5 mg/mL in methanol and water, suggesting transformation into nanofibers (Fig. 1e). UV–Vis, 1H NMR, and FT-IR analyses were conducted to clarify how the molecules were packaged and the molecular interactions between the gelators. For example, the maximum UV absorbance at 245 nm for L-Phe molecules blue-shifted to 238 nm for L-Phe fibrous assemblies, revealing the presence of J-type π-π aggregations in the supramolecular assemblies. As compared to the monomeric L-Phe in DMSO-d_6, the protons at the periphery of the central benzene core showed obvious upfield shifts in the self-assemblies dispersed in D$_2$O ($\sim$7.86 ppm in DMSO-d_6 and 7.51 ppm in D$_2$O) (Fig. 1g), which was attributed to an increase in electron density caused by π-π stacking between the central benzene rings. Moreover, the FT-IR spectra revealed an amide I band at 1643 cm^{-1} and an amide II band at 1546 cm^{-1} for L-Phe assemblies, suggesting the presence of N–H···O═C hydrogen bonds. Moreover, the N–H stretching vibration at 3295 cm^{-1} confirmed the presence of hydrogen bonds between the amide groups (Fig. 1h). The π-π stacking between the benzene cores and hydrogen bonds between the amide groups synergistically drove the supramolecular assemblies (Fig. 1i).

Nanofiber hydrogels of varying chirality were used to culture hDPSCs. The results of the live/dead assay, as illustrated in Fig. S3a, demonstrated that hDPSCs co-cultured with L-Phe, R-Phe, and D-Phe exhibited high viability. This finding was further supported by additional experimental evidence obtained from the EdU and CCK-8 assays (Figs. S3b–d), which clearly demonstrated that the nanofiber hydrogels had no discernible impact on the metabolic activity and proliferative capacity of hDPSCs.

3.2. Effect of chiral nanofiber hydrogels on the osteogenic differentiation of hDPSCs in vitro

ALP activity is an established phenotypic marker of osteogenic differentiation. After incubation for 5 days, ALP activity was greater in the D-Phe group than the R-Phe group and notably lower in the L-Phe group (Fig. 2a and b). Mineralised nodules indicate osteoblast differentiation. After incubation for 21 days, alizarin red S staining and quantification indicated that mineral deposition was greater in the D-Phe group than the R-Phe group and comparatively reduced in the L-Phe group (Fig. 2c and d).

The effects of nanofiber hydrogels on the expression profiles of genes associated with osteogenic differentiation were further investigated using qRT-PCR and western blot analyses. As shown in Fig. 2e, the gene expression levels of *DMP-1*, *OSX*, and *RUNX2* were significantly upregulated in the D-Phe group compared to the R-Phe group, while that of the L-Phe group was even lower. Additionally, the expression levels of *DMP-1* and *OSX* were elevated in the R-Phe group compared with those in the control group. In addition, *RUNX2* gene levels were significantly
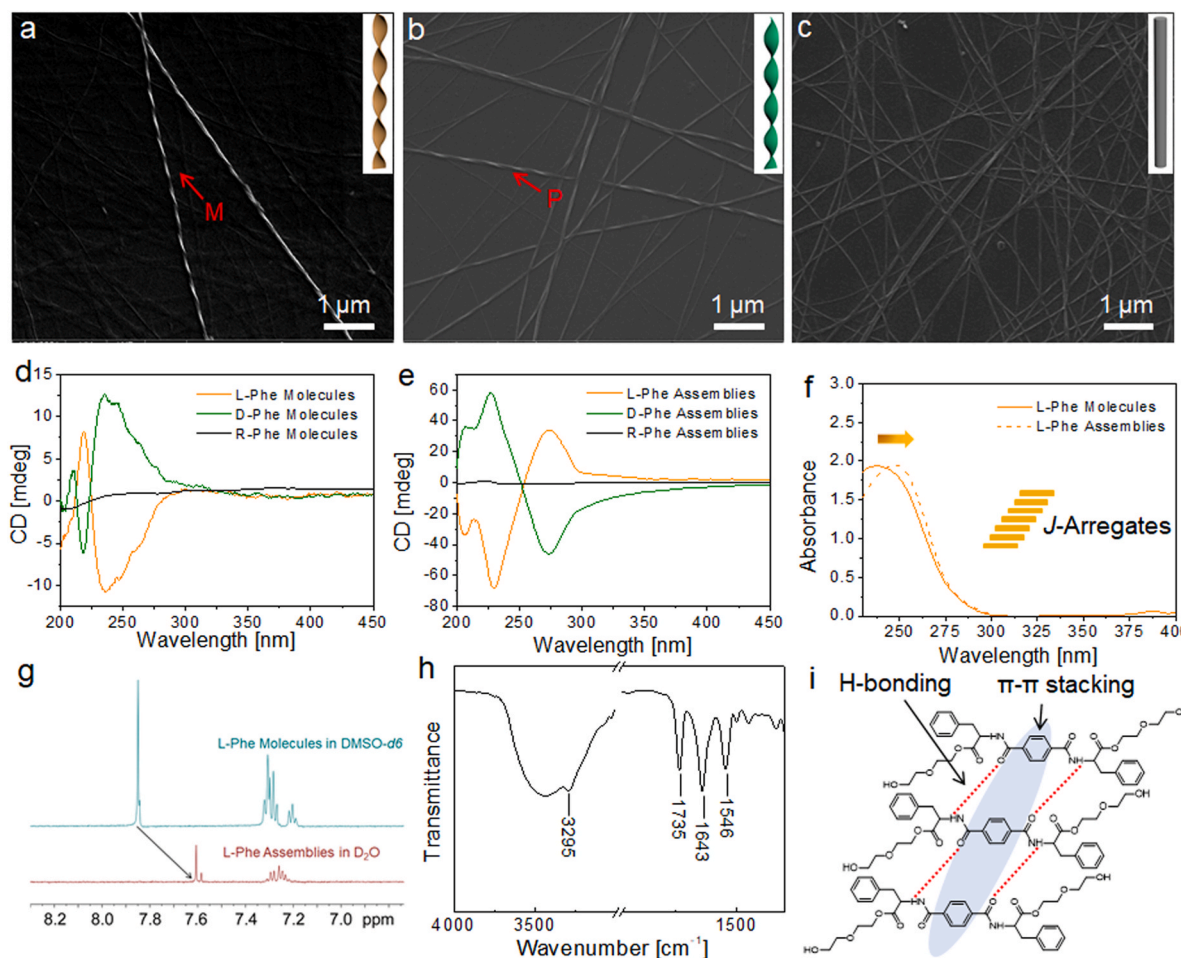
Fig. 1. The characterization of chiral fibrous hydrogels. a. SEM image of left-handed fibers obtained from diluted L-Phe hydrogel (final concentration: 0.1 mg/mL). b. SEM image of right-handed fibers obtained from diluted D-Phe hydrogel (final concentration: 0.1 mg/mL). c. SEM image of non-helical fibers obtained from diluted R-Phe hydrogel (final concentration: 0.1 mg/mL). d. CD spectra of L-Phe, D-Phe, and R-Phe molecules in methanol. e. CD spectra of L-Phe, D-Phe, and R-Phe assemblies in water. f. UV–Vis spectra of L-Phe molecules in methanol and L-Phe assemblies in water. g. 1H NMR spectra of L-Phe molecules in methanol and L-Phe assemblies in water. h. FT-IR spectrum of dried L-Phe chiral hydrogel powder. i. H-bonding and π-π stacking formed between gelators.

reduced in the R-Phe group compared to those in the control group. As shown in Fig. 2f and g, *DMP-1* and *RUNX2* protein levels were significantly up-regulated in the D-Phe group compared to both R-Phe group and control group. Meanwhile, no significant difference was observed in *OSX* protein levels.

3.3. Post-implantation evaluation with a micro-CT system

In addition to evaluating the effects of the chiral matrices on hDPSC differentiation *in vitro*, the potential of hDPSCs combined with chiral matrices to promote tissue regeneration was investigated *in vivo*. Briefly, hDPSCs integrated into chiral matrices were injected into newly formed cranial defects of SD rats. As a control, hDPSCs were injected with saline solution. A micro-CT system was used to quantitatively assess the newly developed bone (BV/TV, BMD, and Tb.Sp). After 8 weeks, the D-Phe group a higher degree of new bone development, BMD, and mineralisation as compared to the control group ($p < 0.05$; Fig. 3a and b), while there were no significant differences between L-Phe and R-Phe groups. Furthermore, BMD was significantly greater in the D-Phe group than in the R-Phe group. As shown in Fig. 3c, serial fluorescence analysis revealed greater new bone formation and mineralisation at 1, 3, and 5 weeks in the D-Phe group compared to the control and R-Phe groups.

3.4. Post-implantation evaluation by bone histomorphometry

The results of HE staining (Fig. 4a) and Van Gieson staining (Fig. 4b) illustrated significant increases in the mineralised area, number of blood vessels, and mature bone tissue in the D-Phe group compared to the R-Phe group. These findings emphasise the superior bone regeneration potential of D-Phe relative to R-Phe at the defect site, underscoring the potential of D-Phe to promote tissue regeneration successfully.

3.5. Identification of key genes and pathways of hDPSCs by integrated bioinformatics

To gain deeper insight into the underlying mechanisms, RNA-seq analysis was conducted. The results of the hierarchical clustering analysis showed distinct gene expression profiles between the L-Phe and D-Phe matrices (Fig. 5a–c). KEGG pathway enrichment analysis of the differentially expressed proteins revealed that the signalling pathways associated with tight junctions were mainly enriched in the L-Phe group, whereas the signalling pathways associated with calcium ion signalling, fatty acid metabolism, and gap junctions were significantly enriched in the D-Phe group. Myosin heavy chain 15 (*MYH15*), adenosine A2A receptor (*ADORA2A*), 5-hydroxytryptamine receptor 2B (*HTR2B*), and acyl-CoA synthetase bubblegum (*ACSBG*) emerged as significant components of the enriched pathways. *MYH15* is associated with tight junctions, whereas *ADORA2A* and *HTR2B* are involved in calcium
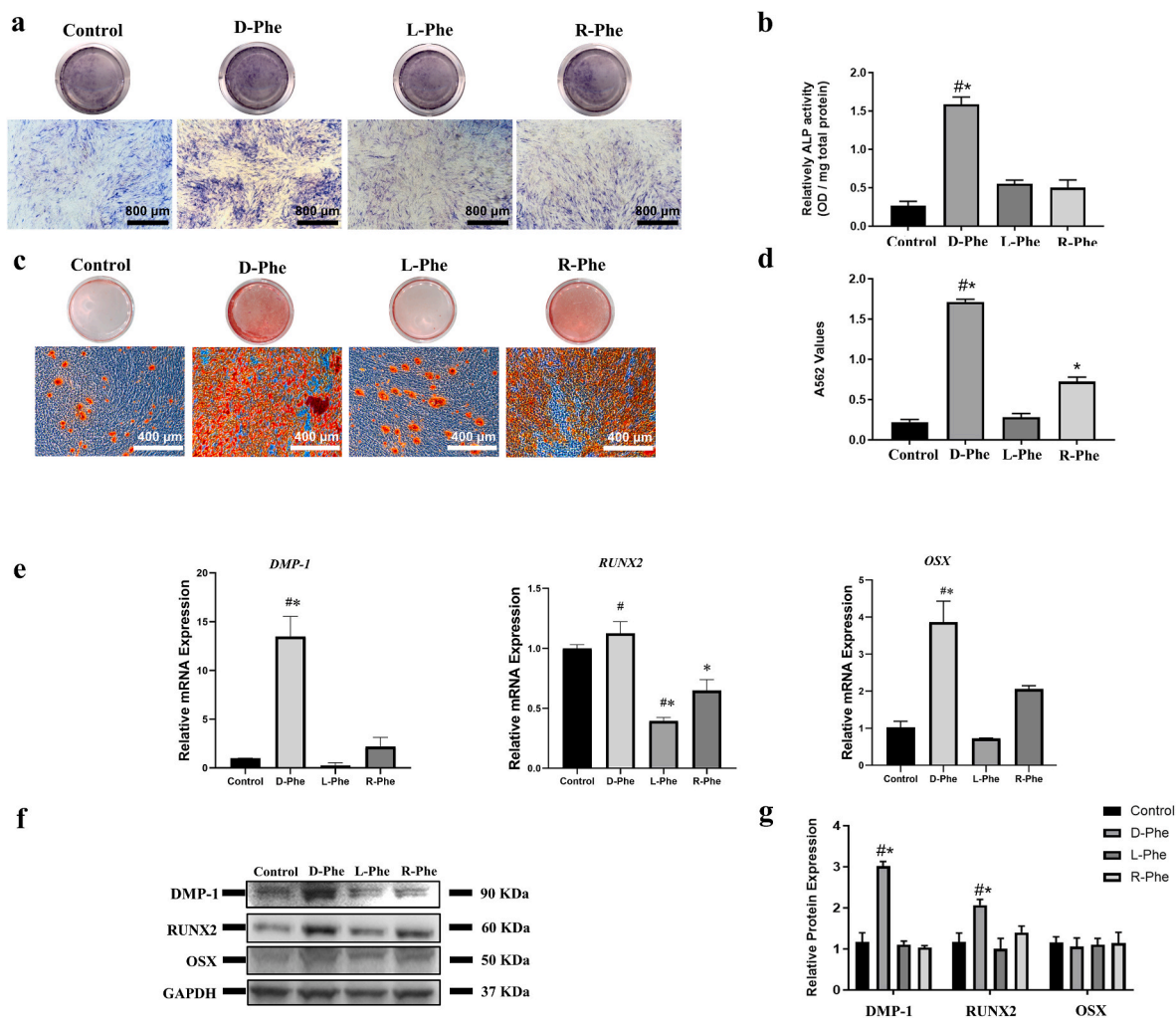
Fig. 2. The effect of chiral nanofiber hydrogels on the osteogenic differentiation of hDPSCs. (a) ALP staining after osteogenic induction of hDPSCs in different chiral environments for 5 days. (b) Quantitative detection of ALP activity of hDPSCs in different chiral environments. (c) Alizarin red staining after osteogenic induction of hDPSCs in different chiral environments for 21 days. (d) Results of semi-quantitative Alizarin red staining assay of hDPSCs in different chiral environments. (e) qRT PCR results of the expression of *DMP-1*, *Runx2* and *OSX* after 3 days of osteogenic induction in different chiral environments of hDPSCs. (f) Western blot results of DMP1, Runx2 and OSX proteins. (g) Quantitative analysis for the ratios of DMP-1, Runx2 and OSX proteins. $*p < 0.05$ versus corresponding control group, $\#p < 0.05$ versus corresponding R-Phe group, one-way analysis of variance (ANOVA) analysis.

signalling. To verify these results, vinculin immunofluorescence staining and a calcium fluorescence probe assay were performed to assess the capacity of hDPSCs to adhere to the nanofiber hydrogels. The immunofluorescence staining results revealed increased vinculin expression in hDPSCs cultured on the L-Phe surface, as well as closer cell-to-cell proximity, in contrast to the cells on the D-Phe surface, which exhibited lower vinculin expression and density (Fig. 6a and b). In addition, the calcium ion fluorescence probe assay revealed markedly higher green fluorescence of the D-Phe group as compared to the L-Phe group, indicating a higher concentration of intracellular calcium (Fig. 6c).

Calcium ions act as intracellular secondary messengers that influence multiple stages of bone regeneration. Thus, pathways associated with calcium ions and involved in cell osteogenesis were identified to explore the role of calcium-related pathways in the osteogenic differentiation of hDPSCs under the regulation of the D-Phe matrix. Briefly, hDPSCs were cultured with or without the different chiral supramolecular hydrogels for 12 h as controls. Western blot analysis showed that *p*-ERK/ERK expression was significantly enhanced in the D-Phe group compared with R-Phe, while there was no significant change to the expression levels of p-p38/pP38 ratio, *p*-JNK/JNK (Fig. 6d and e).

4. Discussion

Previous studies have shown that hDPSCs for BTE are abundant, easily accessible, can be harvested with minimal invasiveness, and grow efficiently in culture [42,43]. Accumulating evidence indicates that the microenvironment influences the fate of hDPSCs by regulating signalling pathways and genes associated with differentiation [18,43]. The development of functional hydrogel scaffolds that mimic ECM is a promising strategy for BTE. Chiral supramolecular hydrogels have superior potential for tissue regeneration compared to traditional polymer hydrogels as bone substitutes, mainly because of their excellent biocompatibility, dynamic noncovalent interactions, and ability to self-assemble into 3D structures [44]. Chirality affects MSCs development and functions of MSCs [30]. Hence, the elucidation of the mechanisms underlying the regulation of chirality and functional differentiation of SCs is fundamental. Therefore, this study aims to systematically investigate the effects of chiral supramolecular hydrogels on the proliferation, differentiation, and adhesion of hDPSCs. This is the first attempt to utilise the chiral structure of the extracellular microenvironment to induce the osteogenic differentiation of hDPSCs. Since hDPSCs cultured in a chiral microenvironment have low immunogenicity, good biocompatibility, and the ability to regulate osteogenic
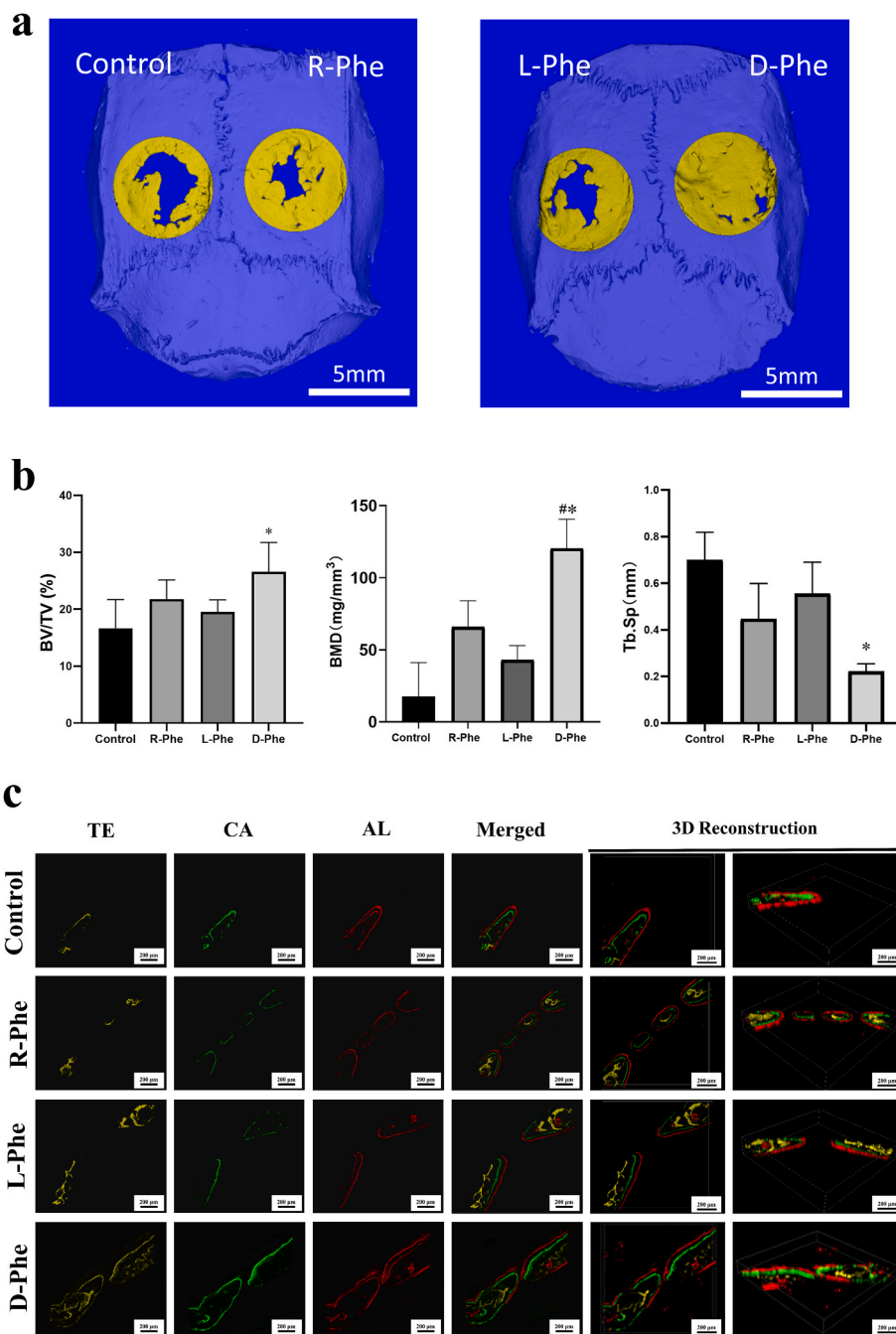
Fig. 3. Micro-CT evaluation of the effect of chiral nanofiber hydrogel on osteogenic potential of hDPSCs, and sequential fluorescent labeling. (a) Grouping and micro-CT reconstruction. (b) Quantitative analysis of bone volume/total volume (BV/TV), bone mineral density (BMD) and bone trabecula space (Tb.Sp) at 8 weeks postoperatively. *$p < 0.05$ versus corresponding control group, #$p < 0.05$ versus corresponding R-Phe group, one-way ANOVA analysis. (c)Sequential fluorescent labeling of Al, TE and Ca was used 1, 3 and 5 weeks after operation.

differentiation, the results of this study offer a novel strategy for the regeneration of craniofacial CSDs.

In the first part of this study, the synthesised chiral supramolecular hydrogel scaffolds were characterised using SEM, CD, UV–Vis, 1H NMR, and FT-IR analyses. Chiral supramolecular hydrogels with fibrous structures mimic the ECM and can be manipulated through the self-assembly of complex supramolecular conformations [45,46]. The biocompatibility of the L-Phe, D-Phe, and R-Phe matrices with encapsulated hDPSCs was confirmed using a live/dead assay (Fig. S3a), EdU assay (Figs. S3b and c), and CCK-8 assay (Fig. S3d). Collectively, these results strongly indicate that the L-Phe, R-Phe, and D-Phe matrices exhibited similar biocompatibility with hDPSCs.

The main objective of using biomimetic scaffold materials for BTE is to promote the osteogenic differentiation of MSCs to replace damaged tissue. A previous study by our group found that commercial hydrogel scaffolds combined with hDPSCs facilitated the repair of mandibular defects in rats [38]. However, because of their inability to directly induce osteogenic differentiation of hDPSCs, commercial hydrogels may affect the regeneration and repair of bone defects to some extent. Notably, the chirality of material surfaces significantly influences the behaviour of MSCs [47]. Chiral hydrogels can simulate the ECM to provide physical support for the multiple physiological activities of MSCs, whereas dynamic and reversible molecular interactions can be exploited to promote tissue reconstruction and formation [44]. Hence,
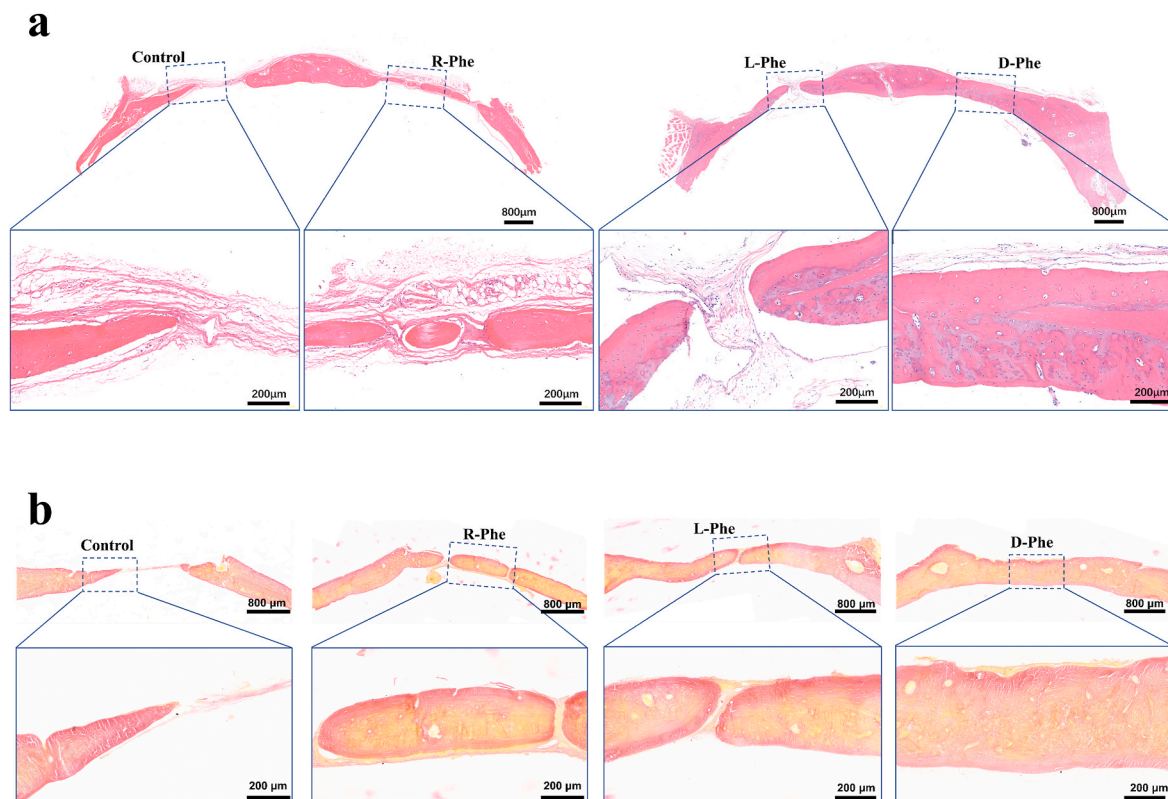
Fig. 4. Histological analysis of newly formed structures after the hydrogels were implanted in defect areas for 8 weeks. (a) HE staining results of full-thickness cranial defect samples. (b) VG staining results.

the development of supramolecular hydrogels with controllable chiral molecular structures and elaborate helical nanostructures is extremely valuable for BTE applications. Therefore, this study also aimed to provide novel insights into how molecular chirality can be utilised as a potential regulator to stimulate the osteogenic differentiation of hDPSCs and explore their biological effects *in vivo*. The results of the *in vitro* experiments demonstrated that the D-Phe group exhibited stronger ALP activity, greater mineral deposition, and higher expression of osteogenesis-related genes and proteins as compared to the R-Phe group. These results indicate that the D-Phe scaffold provides superior osteogenic differentiation of hDPSCs compared to the R- and L-Phe scaffolds, in agreement with the findings of previous studies demonstrating that materials with right-handed helices promote osteogenic differentiation of MSCs better than those with left-handed helices [14]. Yao et al. developed a monolayer cysteine membrane on a material surface with different chiral characteristics (L-/D-Cys-treated groups) that could regulate the differentiation of BMSCs. Following the co-induction of osteogenesis and adipogenesis, a considerable number of BMSCs on the surface of the D-Cys-treated scaffold were transformed into osteoblasts, whereas adipogenesis was greater on the surface of the L-Cys-treated scaffold. The results of the current study regarding chirality-mediated osteogenic differentiation of MSCs are consistent with those of a previous report [14]. In contrast to MSCs cultured on two-dimensional chiral substrates, a 3D ECM-mimetic chiral microenvironment was constructed. In addition, a rat model of CSDs was used to evaluate the bone repair and regeneration capabilities of chiral supramolecular hydrogels loaded with hDPSCs, which is more relevant to clinical settings. The rat model of CSDs confirmed the superior capacity of the D-Phe scaffold loaded with hDPSCs for rapid bone remodelling and formation compared to the L-Phe or R-Phe groups. Indeed, the radiological and histological results confirmed the superiority of the D-Phe scaffold loaded with hDPSCs for bone regeneration. While chirality-mediated multilineage differentiation abilities are distinct from those previously

reported for BMSCs, Wei et al. found that L-Phe chiral molecules favour osteogenesis and D-Phe chiral molecules favour adipogenesis [30]. This discrepancy may be owing to the different sources of SCs and the use of different indicators. Moreover, recent studies on the regulation of SCs by chiral biomaterials found that right-handed DPG nanofibers efficiently facilitated the migration, neuronal differentiation, and synapse formation of retinal progenitor cells compared with left-handed LPG nanofibers [48].

After establishing the crucial role of the 3D chiral microenvironment in regulating the fate of hDPSCs and bone regeneration, the effects of the niche on hDPSCs were investigated. The proliferation and differentiation of MSCs can be influenced by chemical signalling and physical cues [49–51]. Even in the absence of specific chemical signals, other factors such as stress, matrix stiffness, surface adhesion, and micro/-nanomorphology can affect cell morphology [52,53].

RNA-seq analysis revealed significant expression of *MYH15* in the L-Phe group, suggesting that left-handed spiral nanofibers enhanced cell adhesion, which was subsequently confirmed by immunofluorescence staining of vinculin. Adhesive capacity can alter the morphology of MSCs by influencing cell density, which plays a crucial role in regulating intercellular signal transduction and cell differentiation [54]. High-density cell culture promotes intercellular contact and affects cell proliferation and differentiation [55]. Yao et al. reported that materials with left-handed characteristics promote the adhesive and proliferative capacities of BMSCs, resulting in higher cell density, relatively compact morphology, and a tendency towards lipogenic differentiation [14]. However, the capacity of the L-Phe hydrogels to facilitate adipogenic differentiation of hDPSCs was not examined in this study; thus, further investigation is needed. The RNA-seq results also demonstrated that expression of *ACSBG1*, which is related to fatty acid metabolism, was upregulated in the D-Phe group.

Nutritional microenvironment plays a vital role in determining MSCs differentiation and proliferation. Previous studies have established the
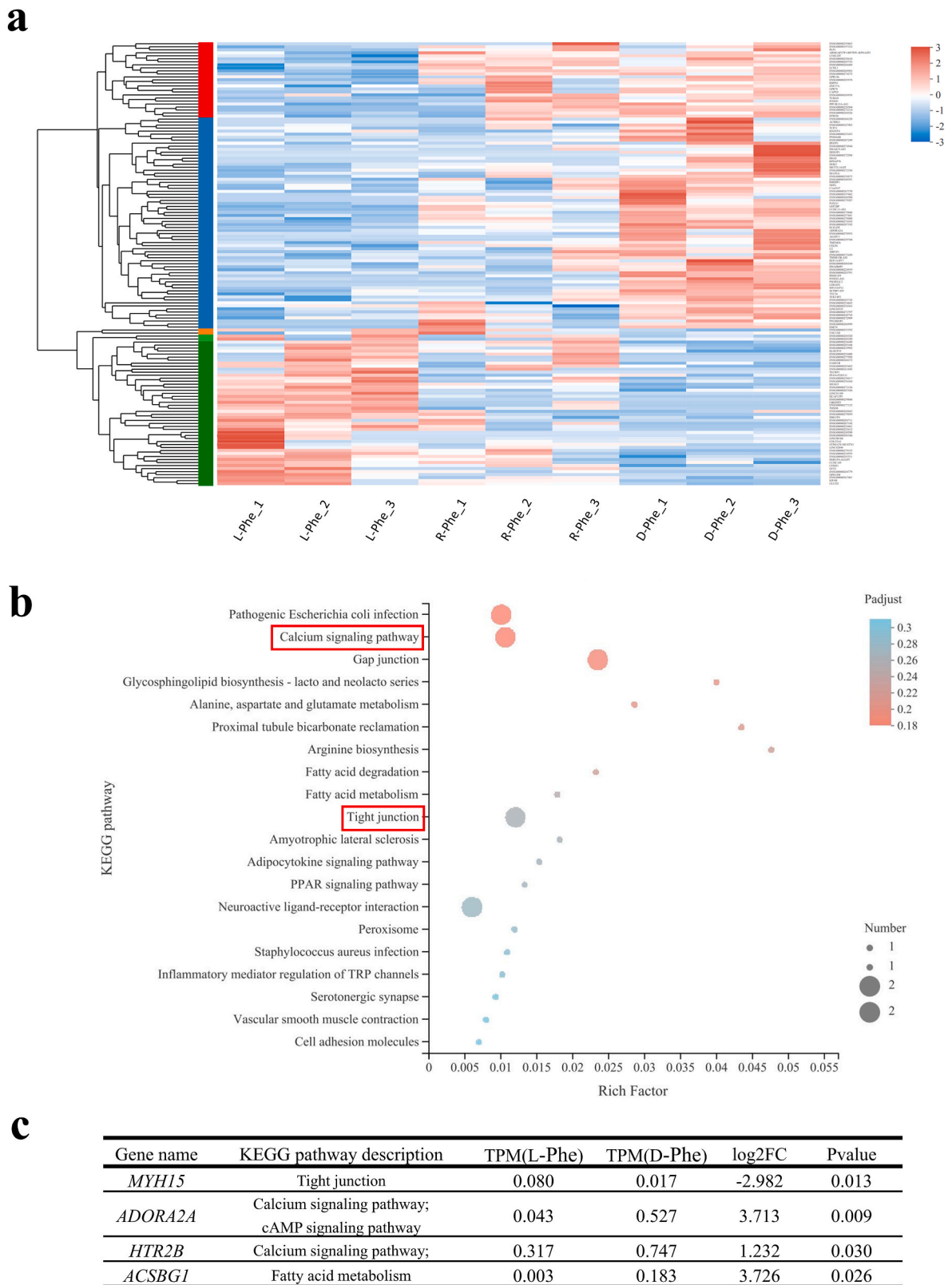
a

b

c

Gene name	KEGG pathway description	TPM(L-Phe)	TPM(D-Phe)	log2FC	Pvalue
MYH15	Tight junction	0.080	0.017	-2.982	0.013
ADORA2A	Calcium signaling pathway; cAMP signaling pathway	0.043	0.527	3.713	0.009
HTR2B	Calcium signaling pathway;	0.317	0.747	1.232	0.030
ACSBG1	Fatty acid metabolism	0.003	0.183	3.726	0.026

Fig. 5. Probing the regulatory landscape of chiral nano-fiber hydrogels on hDPSCs. (a) Clustering heat maps; (b) volcanic map of expression difference; (c) KEGG pathway enrichment analysis.

critical role of fatty acids in bone remodelling [56]. Long-chain fatty acids promote bone metabolism by enhancing osteoblast activity and inhibiting osteoclast activity [57]. Upregulated expression of *ACSBG1* in the D-Phe group suggests that hDPSCs can extract energy from the

surrounding microenvironment, which is a prerequisite for osteogenic differentiation. Additionally, RNA-seq analysis revealed that *ADORA2A*, which is closely linked to osteogenic differentiation of MSCs and maintenance of bone homeostasis [52–54], was significantly
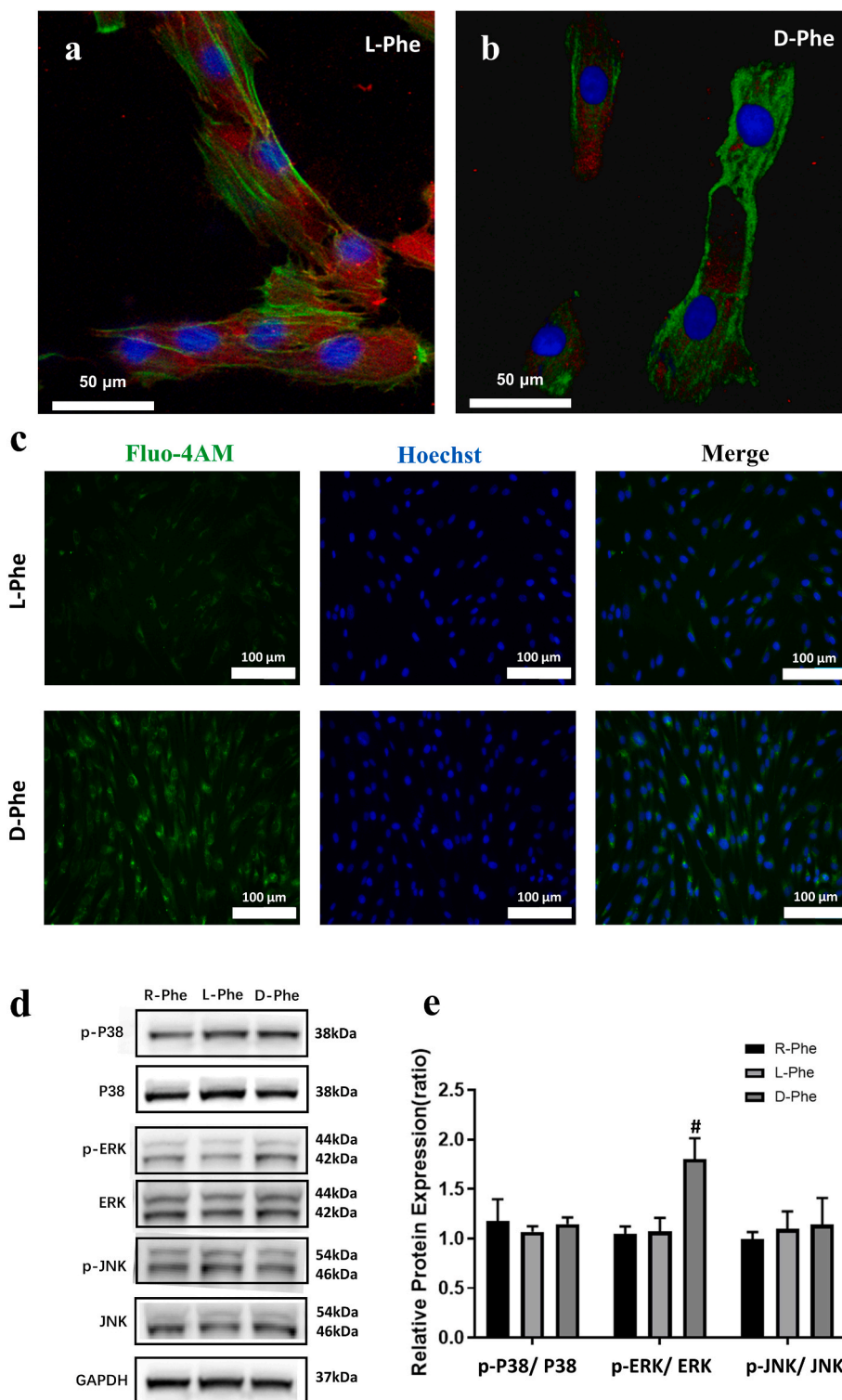
Fig. 6. Cell adhesion on the L-Phe and D-Phe surfaces after 1day of culture. Red: vinculin, green: F-actin, blue: nuclei. (a)Morphology of hDPSCs on L-Phe surface; (b) Morphology of hDPSCs on D-Phe surface. Calcium ion concentration in hDPSCs on the L-Phe and D-Phe surfaces after 1days of culture. Green: Fluo-4AM. Fluorescence microscope images: (c) Morphology of hDPSCs on L-Phe and D-Phe surfaces. (d) Western blot detection of expression of p-P38/P38, *p*-ERK/ERK and *p*-JNK/JNK in hDPSCs. (e) Quantitative analysis for the ratios of p-P38/P38, *p*-ERK/ERK and *p*-JNK/JNK. #p < 0.05 versus corresponding R-Phe group, one-way analysis of variance (ANOVA) analysis.

upregulated in the D-Phe group. Activation of *ADORA2A* can inhibit the activity of osteoclasts while enhancing their differentiation and activity [58,59]. Moreover, the activation of *ADORA2A* promotes the influx of calcium ions into cells [60]. Calcium ions are crucial intracellular secondary messengers that significantly influence multiple stages of bone

regeneration. Notably, calcium ions play a pivotal role in orchestrating the osteogenic differentiation of MSCs [61]. Mechanical forces regulate calcium ion migration through this important transmembrane protein, which is integral to the osteogenic differentiation of MSCs [62]. The D-Phe group exhibited significantly higher green fluorescence than the

L-Phe group, indicating a higher intracellular calcium concentration. This finding was corroborated by the upregulation of *ADORA2A* observed in the RNA-seq analysis. Upregulation of *ADORA2A* activity promotes the influx of calcium ions into hDPSCs, and the associated biological effects are mediated by calmodulin (CaM) binding [63]. Moreover, calmodulin kinase II (CaMKII), which is the main target of the calcium ion/CaM second messenger system [64], is a key regulator of osteoblast differentiation and activates the protein kinase A/MAPK signalling pathway [65] and the subsequent regulation of OSX, thereby promoting the proliferation and osteogenic differentiation of MSCs [66]. Hence, pathways associated with calcium ions and cell osteogenesis were identified to investigate the role of calcium-related pathways in osteogenic differentiation of hDPSCs regulated by the D-Phe matrix. Previous studies have reported that MAPK is involved in the osteogenic/odontogenic differentiation of hDPSCs [67–69]. The results of the current study showed that *p*-ERK levels were significantly increased in the D-Phe group, suggesting that the chiral effect of D-Phe on the osteogenic differentiation of hDPSCs might be mediated by the *p*-ERK/-MAPK pathway. However, further studies are required to elucidate these specific regulatory mechanisms fully.

5. Conclusion

In this study, 3D supramolecular hydrogels constructed from enantiomeric L/D-phenylalanine derivatives were used to investigate the effects of chirality on the osteogenic differentiation of hDPSCs. The results revealed that the D-Phe hydrogel promoted osteogenic differentiation to a greater extent than the L-Phe hydrogel, which could be attributed to an increase in intracellular calcium ion concentrations and activation of the MAPK pathway. Although the precise mechanisms underlying the influence of chiral nanofibers on hDPSCs remain to be fully elucidated, the results of this study offer valuable insights into *in vivo* regulation of differentiation and subsequent osteogenesis of hDPSCs for tissue regeneration and repair of craniofacial tissue defects.

Ethical approval

The study protocols were reviewed and approved by the Ethics Committee of the Ninth People's Hospital affiliated with the Shanghai Jiao Tong University School of Medicine (Shanghai, China) (approval no. SH9H-2021-TK171-1). All experiments involving SD rats were approved by the Institutional Animal Care and Use Committee of the Ninth People's Hospital affiliated with the Shanghai Jiao Tong University School of Medicine.

Funding

CRediT authorship contribution statement

Peilun Li: Writing – review & editing, Writing – original draft, Visualization, Validation, Supervision, Software, Resources, Project administration, Methodology, Investigation, Formal analysis, Data curation, Conceptualization. **Qiaoqiao Jin:** Writing – review & editing, Writing – original draft, Visualization, Validation, Supervision, Software, Resources, Project administration, Methodology, Investigation, Funding acquisition, Formal analysis, Data curation, Conceptualization. **Kangrui Zeng:** Software, Resources, Investigation, Formal analysis, Data curation, Conceptualization. **Chenguang Niu:** Writing – review & editing, Writing – original draft, Validation. **Qianyang Xie:** Formal analysis, Data curation, Conceptualization. **Ting Dong:** Writing – review & editing, Writing – original draft, Resources, Conceptualization. **Zhengwei Huang:** Writing – review & editing, Writing – original draft, Visualization, Validation, Supervision, Software, Resources, Project administration, Methodology, Investigation, Funding acquisition, Formal analysis, Data curation, Conceptualization. **Xiaoqiu Dou:** Writing – review & editing, Writing – original draft, Visualization, Validation, Supervision, Software, Resources, Project administration, Methodology, Investigation, Funding acquisition, Formal analysis, Data curation, Conceptualization. **Chuanliang Feng:** Writing – review & editing, Writing – original draft, Visualization, Validation, Supervision, Software, Resources, Project administration, Methodology, Investigation, Funding acquisition, Formal analysis, Data curation, Conceptualization.

Declaration of competing interest

The authors declare that they have no known competing financial interests or personal relationships that could have appeared to influence the work reported in this paper.

Data availability

No data was used for the research described in the article.

Appendix A. Supplementary data

Supplementary data to this article can be found online at https://doi.org/10.1016/j.mtbio.2024.100971.

References

[1] Z.M. Johnson, Y. Yuan, X. Li, T. Jashashvili, M. Jamieson, M. Urata, Y. Chen, Y. Chai, Mesenchymal stem cells and three-dimensional-osteoconductive scaffold regenerate calvarial bone in critical size defects in swine, Stem cells translational medicine 10 (8) (2021) 1170–1183, https://doi.org/10.1002/sctm.20-0534.

[2] C. Cordonnier, A. Demchuk, W. Ziai, C.S. Anderson, Intracerebral haemorrhage: current approaches to acute management, Lancet (London, England) 392 (10154) (2018) 1257–1268, https://doi.org/10.1016/s0140-6736(18)31878-6.

[3] E. Mazzoni, M.R. Iaquinta, M. Mosaico, R. De Pace, A. D'Agostino, M. Tognon, F. Martini, Human Mesenchymal Stem Cells and Innovative Scaffolds for Bone Tissue Engineering Applications, Tissue Engineering, Part B, Reviews, 2023, https://doi.org/10.1089/ten.TEB.2022.0217.

[4] S.M. Gronthos, M, J. Brahim, P.G. Robey, S. Shi, Postnatal human dental pulp stem cells (DPSCs) in vitro and in vivo, Proc. Natl. Acad. Sci. U. S. A. 97 (25) (2000) 13625–13630, https://doi.org/10.1073/pnas.240309797.

[5] S. Gronthos, J. Brahim, W. Li, L.W. Fisher, N. Cherman, A. Boyde, P. DenBesten, P. G. Robey, S. Shi, Stem cell properties of human dental pulp stem cells, J. Dent. Res. 81 (8) (2002) 531–535, https://doi.org/10.1177/154405910208100806.

[6] J. Lyu, Y. Hashimoto, Y. Honda, N. Matsumoto, Comparison of osteogenic potentials of dental pulp and bone marrow mesenchymal stem cells using the new cell transplantation platform, CellSaic, in a rat congenital cleft-jaw model, Int. J. Mol. Sci. 22 (17) (2021), https://doi.org/10.3390/ijms22179478.

[7] Y. Yamada, S. Nakamura-Yamada, K. Kusano, S. Baba, Clinical potential and current progress of dental pulp stem cells for various systemic Diseases in regenerative medicine: a concise review, Int. J. Mol. Sci. 20 (5) (2019), https://doi.org/10.3390/ijms20051132.

[8] D.L. Alge, D. Zhou, L.L. Adams, B.K. Wyss, M.D. Shadday, E.J. Woods, T.M. Gabriel Chu, W.S. Goebel, Donor-matched comparison of dental pulp stem cells and bone

marrow-derived mesenchymal stem cells in a rat model, J Tissue Eng Regen Med 4 (1) (2010) 73–81, https://doi.org/10.1002/term.220.

[9] Y.C. Lee, Y.H. Chan, S.C. Hsieh, W.Z. Lew, S.W. Feng, Comparing the osteogenic potentials and bone regeneration capacities of bone marrow and dental pulp mesenchymal stem cells in a rabbit calvarial bone defect model, Int. J. Mol. Sci. 20 (20) (2019), https://doi.org/10.3390/ijms20205015.

[10] Q. Jin, P. Li, K. Yuan, F. Zhao, X. Zhu, P. Zhang, Z. Huang, Extracellular vesicles derived from human dental pulp stem cells promote osteogenesis of adipose-derived stem cells via the MAPK pathway, J. Tissue Eng. 11 (2020) 2041731420975569, https://doi.org/10.1177/2041731420975569.

[11] J.F. Huo, M.L. Zhang, X.X. Wang, D.H. Zou, Chrysin induces osteogenic differentiation of human dental pulp stem cells, Exp. Cell Res. 400 (2) (2021) 112466, https://doi.org/10.1016/j.yexcr.2020.112466.

[12] Y.-H. Chan, K.-N. Ho, Y.-C. Lee, M.-J. Chou, W.-Z. Lew, H.-M. Huang, P.-C. Lai, S.-W. Feng, Melatonin enhances osteogenic differentiation of dental pulp mesenchymal stem cells by regulating MAPK pathways and promotes the efficiency of bone regeneration in calvarial bone defects, Stem Cell Res. Ther. 13 (1) (2022), https://doi.org/10.1186/s13287-022-02744-z.

[13] R. Oliveira É, L. Nie, D. Podstawczyk, A. Allahbakhsh, J. Ratnayake, D.L. Brasil, A. Shavandi, Advances in growth factor delivery for bone tissue engineering, Int. J. Mol. Sci. 22 (2) (2021), https://doi.org/10.3390/ijms22020903.

[14] X. Yao, Y. Hu, B. Cao, R. Peng, J. Ding, Effects of surface molecular chirality on adhesion and differentiation of stem cells, Biomaterials 34 (36) (2013) 9001–9009, https://doi.org/10.1016/j.biomaterials.2013.08.013.

[15] H. Zheng, T. Yoshitomi, K. Yoshimoto, Analysis of chirality effects on stem cell fate using three-dimensional fibrous peptide hydrogels, ACS Appl. Bio Mater. 1 (3) (2018) 538–543, https://doi.org/10.1021/acsabm.8b00123.

[16] Y. Li, Y. Xiao, C. Liu, The horizon of materiobiology: a perspective on material-guided cell behaviors and tissue engineering, Chem. Rev. 117 (5) (2017) 4376–4421, https://doi.org/10.1021/acs.chemrev.6b00654.

[17] A. Baran, M. Fırat Baran, C. Keskin, A. Hatipoğlu, Ö. Yavuz, S. İrtegün Kandemir, M.T. Adican, R. Khalilov, A. Mammadova, E. Ahmadian, G. Rosić, D. Selakovic, A. Eftekhari, Investigation of antimicrobial and cytotoxic properties and specification of silver nanoparticles (AgNPs) derived from cicer arietinum L. Green leaf extract, Front. Bioeng. Biotechnol. 10 (2022) 855136, https://doi.org/10.3389/fbioe.2022.855136.

[18] G. Brunello, F. Zanotti, G. Scortecci, L. Sapoznikov, S. Sivolella, B. Zavan, Dentin particulate for bone regeneration: an in vitro study, Int. J. Mol. Sci. 23 (16) (2022), https://doi.org/10.3390/ijms23169283.

[19] M. Tatullo, M. Marrelli, G. Falisi, C. Rastelli, F. Palmieri, M. Gargari, B. Zavan, F. Paduano, V. Benagiano, Mechanical influence of tissue culture plates and extracellular matrix on mesenchymal stem cell behavior: a topical review, Int. J. Immunopathol. Pharmacol. 29 (1) (2016) 3–8, https://doi.org/10.1177/0394632015617951.

[20] E. Ahmadian, A. Eftekhari, D. Janas, P. Vahedi, Nanofiber scaffolds based on extracellular matrix for articular cartilage engineering: a perspective, Nanotheranostics 7 (1) (2023) 61–69, https://doi.org/10.7150/ntno.78611.

[21] S. Shahi, F. Dehghani, E.D. Abdolahinia, S. Sharifi, E. Ahmadian, M. Gajdács, K. Kárpáti, S.M. Dizaj, A. Eftekhari, T. Kavetskyy, Effect of gelatinous spongy scaffold containing nano-hydroxyapatite on the induction of odontogenic activity of dental pulp stem cells, J. King Saud Univ. Sci. 34 (8) (2022) 102340, https://doi.org/10.1016/j.jksus.2022.102340.

[22] S. Utsunomiya, S. Sakamura, T. Sasamura, T. Ishibashi, C. Maeda, M. Inaki, K. Matsuno, Cells with broken left–right symmetry: roles of intrinsic cell chirality in left–right asymmetric epithelial morphogenesis, Symmetry 11 (4) (2019), https://doi.org/10.3390/sym11040505.

[23] M. Inaki, T. Sasamura, K. Matsuno, Cell chirality drives left-right asymmetric morphogenesis, Front. Cell Dev. Biol. 6 (2018) 34, https://doi.org/10.3389/fcell.2018.00034.

[24] F. Zhou, L. Yuan, D. Li, H. Huang, T. Sun, H. Chen, Cell adhesion on chiral surface: the role of protein adsorption, Colloids Surf. B Biointerfaces 90 (2012) 97–101, https://doi.org/10.1016/j.colsurfb.2011.10.016.

[25] X. Dou, N. Mehwish, C. Zhao, J. Liu, C. Xing, C. Feng, Supramolecular hydrogels with tunable chirality for promising biomedical applications, Acc. Chem. Res. 53 (4) (2020) 852–862, https://doi.org/10.1021/acs.accounts.0c00012.

[26] B. Chang, N. Ahuja, C. Ma, X. Liu, Injectable scaffolds: preparation and application in dental and craniofacial regeneration, Materials science & engineering, R, Reports : a review journal 111 (2017) 1–26, https://doi.org/10.1016/j.mser.2016.11.001.

[27] Y. Wang, Y. Yang, X. Wang, T. Yoshitomi, N. Kawazoe, Y. Yang, G. Chen, Micropattern-controlled chirality of focal adhesions regulates the cytoskeletal arrangement and gene transfection of mesenchymal stem cells, Biomaterials 271 (2021) 120751, https://doi.org/10.1016/j.biomaterials.2021.120751.

[28] X. Zhao, S.Q. Zang, X. Chen, Stereospecific interactions between chiral inorganic nanomaterials and biological systems, Chem. Soc. Rev. 49 (8) (2020) 2481–2503, https://doi.org/10.1039/d0cs00093k.

[29] Y. Bao, S. Wu, L.T. Chu, H.K. Kwong, Y. Huang, M.L. Lam, R.H. W. Lam, T.H. Chen, Early committed clockwise cell chirality upregulates adipogenic differentiation of mesenchymal stem cells, Adv Biosyst 4 (10) (2020) e2000161, https://doi.org/10.1002/adbi.202000161.

[30] Y. Wei, S. Jiang, M. Si, X. Zhang, J. Liu, Z. Wang, C. Cao, J. Huang, H. Huang, L. Chen, S. Wang, C. Feng, X. Deng, L. Jiang, Chirality controls mesenchymal stem cell lineage diversification through mechanoresponses, Adv. Mater. 31 (16) (2019) e1900582, https://doi.org/10.1002/adma.201900582.

[31] X. Dou, B. Wu, J. Liu, C. Zhao, M. Qin, Z. Wang, H. Schonherr, C. Feng, Effect of chirality on cell spreading and differentiation: from chiral molecules to chiral self-

[32] assembly, ACS Appl. Mater. Interfaces 11 (42) (2019) 38568–38577, https://doi.org/10.1021/acsami.9b15710.

[32] G.F. Liu, D. Zhang, C.L. Feng, Control of three-dimensional cell adhesion by the chirality of nanofibers in hydrogels, Angew Chem. Int. Ed. Engl. 53 (30) (2014) 7789–7793, https://doi.org/10.1002/anie.201403249.

[33] S. Wang, L. Gao, N. Su, L. Yang, F. Gao, X. Dou, C. Feng, Inversion of supramolecular chirality by in situ hydrolyzation of achiral diethylene glycol motifs, J. Phys. Chem. B 126 (6) (2022) 1325–1333, https://doi.org/10.1021/acs.jpcb.1c10018.

[34] J. Liu, F. Yuan, X. Ma, D.i.Y. Auphedeous, C. Zhao, C. Liu, C. Shen, C. Feng, The cooperative effect of both molecular and supramolecular chirality on cell adhesion, Angew. Chem. Int. Ed. 57 (22) (2018) 6475–6479, https://doi.org/10.1002/anie.201801462.

[35] N. Sun, X. Dou, Z. Tang, D. Zhang, N. Ni, J. Wang, H. Gao, Y. Ju, X. Dai, C. Zhao, P. Gu, J. Ji, C. Feng, Bio-inspired chiral self-assemblies promoted neuronal differentiation of retinal progenitor cells through activation of metabolic pathway, Bioact. Mater. 6 (4) (2021) 990–997, https://doi.org/10.1016/j.bioactmat.2020.09.027.

[36] Z. Shen, S. Kuang, Y. Zhang, M. Yang, W. Qin, X. Shi, Z. Lin, Chitosan hydrogel incorporated with dental pulp stem cell-derived exosomes alleviates periodontitis in mice via a macrophage-dependent mechanism, Bioact. Mater. 5 (4) (2020) 1113–1126, https://doi.org/10.1016/j.bioactmat.2020.07.002.

[37] N. Su, C. Villicana, D. Barati, P. Freeman, Y. Luo, F. Yang, Stem cell membrane-coated microribbon scaffolds induce regenerative innate and adaptive immune responses in a critical-size cranial bone defect model, Adv. Mater. 35 (10) (2023) e2208781, https://doi.org/10.1002/adma.202208781.

[38] Q. Jin, K. Yuan, W. Lin, C. Niu, R. Ma, Z. Huang, Comparative characterization of mesenchymal stem cells from human dental pulp and adipose tissue for bone regeneration potential, Artif. Cells, Nanomed. Biotechnol. 47 (1) (2019) 1577–1584, https://doi.org/10.1080/21691401.2019.1594861.

[39] B. Li, C.N. Dewey, RSEM: accurate transcript quantification from RNA-Seq data with or without a reference genome, BMC Bioinf. 12 (2011) 323, https://doi.org/10.1186/1471-2105-12-323.

[40] S. Shen, J.W. Park, Z.X. Lu, L. Lin, M.D. Henry, Y.N. Wu, Q. Zhou, Y. Xing, rMATS: robust and flexible detection of differential alternative splicing from replicate RNA-Seq data, Proc. Natl. Acad. Sci. U. S. A 111 (51) (2014) E5593–E5601, https://doi.org/10.1073/pnas.1419161111.

[41] X. Dou, B. Wu, J. Liu, C. Zhao, M. Qin, Z. Wang, H. Schönherr, C. Feng, Effect of chirality on cell spreading and differentiation: from chiral molecules to chiral self-assembly, ACS Appl. Mater. Interfaces 11 (42) (2019) 38568–38577, https://doi.org/10.1021/acsami.9b15710.

[42] A. Ariano, F. Posa, G. Storlino, G. Mori, Molecules inducing dental stem cells differentiation and bone regeneration: state of the art, Int. J. Mol. Sci. 24 (12) (2023), https://doi.org/10.3390/ijms24129897.

[43] A. Namjoynik, M.A. Islam, M. Islam, Evaluating the efficacy of human dental pulp stem cells and scaffold combination for bone regeneration in animal models: a systematic review and meta-analysis, Stem Cell Res. Ther. 14 (1) (2023) 132, https://doi.org/10.1186/s13287-023-03357-w.

[44] X. Wang, C. Feng, Chiral fiber supramolecular hydrogels for tissue engineering, Wiley interdisciplinary reviews, Nanomedicine and nanobiotechnology 15 (2) (2023) e1847, https://doi.org/10.1002/wnan.1847.

[45] M. Tzaphlidou, Bone architecture: collagen structure and calcium/phosphorus maps, J. Biol. Phys. 34 (1–2) (2008) 39–49, https://doi.org/10.1007/s10867-008-9115-y.

[46] X.Q. Dou, C.L. Feng, Amino acids and peptide-based supramolecular hydrogels for three-dimensional cell culture, Adv. Mater. 29 (16) (2017), https://doi.org/10.1002/adma.201604062.

[47] T. Yoshitomi, H. Zheng, K. Yoshimoto, Investigations of chirality effects on undifferentiated state of mesenchymal stem cells using soft nanofibrous oligopeptide hydrogels, Anal. Sci. : the international journal of the Japan Society for Analytical Chemistry 37 (3) (2021) 539–543, https://doi.org/10.2116/analsci.20SCN05.

[48] N. Sun, X. Dou, Z. Tang, D. Zhang, N. Ni, J. Wang, H. Gao, Y. Ju, X. Dai, C. Zhao, P. Gu, J. Ji, C. Feng, Bio-inspired chiral self-assemblies promoted neuronal differentiation of retinal progenitor cells through activation of metabolic pathway, Bioact. Mater. 6 (4) (2021) 990–997, https://doi.org/10.1016/j.bioactmat.2020.09.027.

[49] J. He, N. Zhang, Y. Zhu, R. Jin, F. Wu, MSC spheroids-loaded collagen hydrogels simultaneously promote neuronal differentiation and suppress inflammatory reaction through PI3K-Akt signaling pathway, Biomaterials 265 (2021) 120448, https://doi.org/10.1016/j.biomaterials.2020.120448.

[50] H. Abdelrazik, E. Giordano, G. Barbanti Brodano, C. Griffoni, E. De Falco, A. Pelagalli, Substantial overview on mesenchymal stem cell biological and physical properties as an opportunity in translational medicine, Int. J. Mol. Sci. 20 (21) (2019), https://doi.org/10.3390/ijms20215386.

[51] A.A. Saidova, I.A. Vorobjev, Lineage commitment, signaling pathways, and the cytoskeleton systems in mesenchymal stem cells, tissue engineering, Part B, Reviews 26 (1) (2020) 13–25, https://doi.org/10.1089/ten.TEB.2019.0250.

[52] P. Ghensi, E. Bressan, C. Gardin, L. Ferroni, L. Ruffato, M. Caberlotto, C. Soldini, B. Zavan, Osteo Growth Induction titanium surface treatment reduces ROS production of mesenchymal stem cells increasing their osteogenic commitment, Mater. Sci. Eng., C 74 (2017) 389–398, https://doi.org/10.1016/j.msec.2016.12.032.

[53] L. Ferroni, U. D'Amora, S. Leo, E. Tremoli, M.G. Raucci, A. Ronca, L. Ambrosio, B. Zavan, PEEK and hyaluronan-based 3D printed structures: promising

combination to improve bone regeneration, Molecules 27 (24) (2022), https://doi.org/10.3390/molecules27248749.

[54] G. Le Saux, M.C. Wu, E. Toledo, Y.Q. Chen, Y.J. Fan, J.C. Kuo, M. Schvartzman, Cell-cell adhesion-driven contact guidance and its effect on human mesenchymal stem cell differentiation, ACS Appl. Mater. Interfaces 12 (20) (2020) 22399–22409, https://doi.org/10.1021/acsami.9b20939.

[55] A. Puliafito, L. Hufnagel, P. Neveu, S. Streichan, A. Sigal, D.K. Fygenson, B. I. Shraiman, Collective and single cell behavior in epithelial contact inhibition, Proc. Natl. Acad. Sci. U. S. A 109 (3) (2012) 739–744, https://doi.org/10.1073/pnas.1007809109.

[56] M. Bao, K. Zhang, Y. Wei, W. Hua, Y. Gao, X. Li, L. Ye, Therapeutic potentials and modulatory mechanisms of fatty acids in bone, Cell Prolif. 53 (2) (2020) e12735, https://doi.org/10.1111/cpr.12735.

[57] Y. Liu, M. Tingart, S. Lecouturier, J. Li, J. Eschweiler, Identification of co-expression network correlated with different periods of adipogenic and osteogenic differentiation of BMSCs by weighted gene co-expression network analysis (WGCNA), BMC Genom. 22 (1) (2021) 254, https://doi.org/10.1186/s12864-021-07584-4.

[58] A. Mediero, T. Wilder, V.S. Reddy, Q. Cheng, N. Tovar, P.G. Coelho, L. Witek, C. Whatling, B.N. Cronstein, Ticagrelor regulates osteoblast and osteoclast function and promotes bone formation in vivo via an adenosine-dependent mechanism, Faseb. J. : official publication of the Federation of American Societies for Experimental Biology 30 (11) (2016) 3887–3900, https://doi.org/10.1096/fj.201600616R.

[59] L. Xiong, J.U. Jung, H.H. Guo, J.X. Pan, X.D. Sun, L. Mei, W.C. Xiong, Osteoblastic Lrp4 promotes osteoclastogenesis by regulating ATP release and adenosine-A(2A)R signaling, J. Cell Biol. 216 (3) (2017) 761–778, https://doi.org/10.1083/jcb.201608002.

[60] S.N. Li, P.T. Wong, The adenosine receptor agonist, APNEA, increases calcium influx into rat cortical synaptosomes through N-type channels associated with A2a receptors, Neurochem. Res. 25 (4) (2000) 457–459, https://doi.org/10.1023/a:1007503907823.

[61] F. Viti, M. Landini, A. Mezzelani, L. Petecchia, L. Milanesi, S. Scaglione, Osteogenic differentiation of MSC through calcium signaling activation: transcriptomics and functional analysis, PLoS One 11 (2) (2016) e0148173, https://doi.org/10.1371/journal.pone.0148173.

[62] T. Ma, Q. Ding, C. Liu, H. Wu, Electromagnetic fields regulate calcium-mediated cell fate of stem cells: osteogenesis, chondrogenesis and apoptosis, Stem Cell Res. Ther. 14 (1) (2023) 133, https://doi.org/10.1186/s13287-023-03303-w.

[63] Y.Y. Zhang, J. Yue, H. Che, H.Y. Sun, H.F. Tse, G.R. Li, BKCa and hEag1 channels regulate cell proliferation and differentiation in human bone marrow-derived mesenchymal stem cells, J. Cell. Physiol. 229 (2) (2014) 202–212, https://doi.org/10.1002/jcp.24435.

[64] M. Zayzafoon, Calcium/calmodulin signaling controls osteoblast growth and differentiation, J. Cell. Biochem. 97 (1) (2006) 56–70, https://doi.org/10.1002/jcb.20675.

[65] S. Stewart, A. Darwood, S. Masouros, C. Higgins, A. Ramasamy, Mechanotransduction in osteogenesis, Bone & joint research 9 (1) (2020) 1–14, https://doi.org/10.1302/2046-3758.91.Bjr-2019-0043.R2.

[66] Y. Song, H. Wu, Y. Gao, J. Li, K. Lin, B. Liu, X. Lei, P. Cheng, S. Zhang, Y. Wang, J. Sun, L. Bi, G. Pei, Zinc silicate/nano-hydroxyapatite/collagen scaffolds promote angiogenesis and bone regeneration via the p38 MAPK pathway in activated monocytes, ACS Appl. Mater. Interfaces 12 (14) (2020) 16058–16075, https://doi.org/10.1021/acsami.0c00470.

[67] X. He, W. Jiang, Z. Luo, T. Qu, Z. Wang, N. Liu, Y. Zhang, P.R. Cooper, W. He, IFN-γ regulates human dental pulp stem cells behavior via NF-κB and MAPK signaling, Sci. Rep. 7 (2017) 40681, https://doi.org/10.1038/srep40681.

[68] J. Li, Z. Wang, J. Wang, Q. Guo, Y. Fu, Z. Dai, M. Wang, Y. Bai, X. Liu, P.R. Cooper, J. Wu, W. He, Amphiregulin regulates odontogenic differentiation of dental pulp stem cells by activation of mitogen-activated protein kinase and the phosphatidylinositol 3-kinase signaling pathways, Stem Cell Res. Ther. 13 (1) (2022) 304, https://doi.org/10.1186/s13287-022-02971-4.

[69] Y. Kong, X. Hu, Y. Zhong, K. Xu, B. Wu, J. Zheng, Magnesium-enriched microenvironment promotes odontogenic differentiation in human dental pulp stem cells by activating ERK/BMP2/Smads signaling, Stem Cell Res. Ther. 10 (1) (2019) 378, https://doi.org/10.1186/s13287-019-1493-5.